SCIENTIFIC PAPERS
OF THE UNIVERSITY OF PARDUBICE
Series A
Faculty of Chemical Technology
23 (2017)

INVESTIGATION OF THE STRUCTURAL AND CHARGE PROPERTIES OF A POLYAMIDE NANOFILTRATION MEMBRANE

Edwin WALLACE, Jiří CUHORKA, and Petr MIKULÁŠEK[1]
Institute of Environmental and Chemical Engineering,
The University of Pardubice, CZ–532 10 Pardubice

Received February 15, 2017

Nanofiltration (NF) membrane had gained interest worldwide due to the excellent removal of contaminant(s) with lower energy consumption compared to reverse osmosis. NF is used for several environmental applications; for example, pharmaceutical and biotechnology, or desalination. The fundamental principle behind the separation mechanism of nanofiltration can be fully understood by defining the structural and charge properties of the membrane. In the present work, a polyamide thin-film composite NF membrane (AFC 30) was used for characterization of the structural and charge surface properties. The structural properties are the pore radius (r_p) and the membrane thickness-to-porosity ratio ($\Delta x/A_k$), respectively. The interpretation of values from the different uncharged solutes rejection allows one to determine the structural properties of AFC 30. This was done by using modelling of rejection of the uncharged solutes with the aid of the Donnan steric partitioning model (DSPM). In addition, the membrane was

[1] To whom correspondence should be addressed.

considered to be modelled as a bundle of cylindrical pores. It has been observed that the pore radius and thickness-to-porosity ratio from AFC 30 membrane are similar irrespective of the different uncharged solutes. The fixed charge density on the membrane surface was determined by experiments with sodium chloride at different concentrations. The data from such a sodium chloride experiment(s) were used to calculate the effective charge density (ΦX) by using the Spiegler–Kedem model together with a charge model called Teorell–Meyer–Sievers (TMS). Then, it has been revealed that the membrane charge depends solely on the salt concentration in the solution because of the ion adsorption onto the membrane surface. The reliance of the charge density of the NaCl concentration follows the well-known equation — Freundlich isotherm.

Introduction

Nanofiltration is a subset of a cross flow, representing the pressure-driven process with properties in-between ultrafiltration (UF) and reverse osmosis (RO). It has many interesting environmental applications, such as treatment of ground water, surface water, and waste water reclamation. As compared to the other pressure-driven processes, NF is characterized by a membrane pore size below 1 nm, corresponding to a molecular weight cut off (MWCO) of approximately 200-1 000 Dalton [1]. Nanofiltration offers some advantages compared to reverse osmosis: (i) less energy consumption, (ii) lower operating pressure than RO, (iii) higher flux, (iv) specific permeability, when monovalent ions partly pass through (compared to reverse osmosis, there is a lower rejection of monovalent ions), whereas multivalent ions are rejected to a substantial degree, and (v) inexpensiveness [2]. The membrane can be positively or negatively charged, depending on the material from which is formed. Moreover, the membrane charge is as a result of dissociation of ionizable functional group(s) in the membrane surface and pores. This group can be acidic or basic in nature or a combination of both; again, depending on the material used in manufacturing and fabrication processes. Due to the complex nature, up until now, the separation mechanism is not fully understood [3].

The separation process of NF is a combination of the size exclusion and electrical interaction existing between the ions in the feed solution and the charged NF membrane. For prediction and separation of NF, it is paramount to understand the characterization of NF material for practical use [4]. This can be achieved by determining the structural properties and charge of the membrane. The structural properties refer to the pore size and the membrane thickness-to-porosity ratio. Rejection of a solute is a result of the membrane pore size. The flux is influenced by the pore size and membrane thickness to porosity [5]. At present, atomic force microscopy (AFM) is being used for direct measurement of the structural

properties, but this technique does not give a very precise reading of NF membrane. The reason is that the pores are generally very small and also the respective AFM images of the membrane surface cannot provide sufficient information about the structure of the pores inside the membrane. Likewise, other approaches used to estimate the membrane charge density, such as electrokinetic measurement, evaluation of membrane potential or of ion-exchange capacity usually give qualitative information [6] and help to define the transport of the solute in NF membrane.

Many models have been developed for prediction and performance of the NF membrane due to the separation mechanism. These models are used to describe and predict the flux as well as the retention of both uncharged and charged species at the NF membrane under different operational conditions. The mathematical models can be divided into several classes; namely, non-equilibrium thermodynamic (IT) model, pore models and non-porous models. Numerous hypotheses proposed so far were based on either structural parameters or electrical (charged) properties of the membrane [3,7]. Most often, membrane characteristics (pore size, membrane thickness-to-porosity ratio) are analyzed by the uncharged solutes and salt retention experiments using the proper structure models, such as the Donnan steric partitioning model (DSPM) [8,9], Spiegler–Kedem model or in combination with steric-hindrance pore model (SHP) [10,11]. Other complex models like Teorell–Meyer–Sievers (TMS) model [12], space charge (SC) [13], electrostatic and steric hindrance (ES) model [7], DSPM with dielectric exclusion (DSPM-DE) model [9,14], steric, electric, and dielectric exclusion (SEDE) models [10,15] have also been proposed. A generally known technique used to determine the characterization of the membrane is being based on the rejection experiments of uncharged solutes and then on the use of different mathematical models to estimate the pore size (r_p) and the membrane thickness-to-porosity ratio ($\Delta x/A_k$). The electrical properties of the membrane can be described by estimating the charge density of the membrane by means of the Teorell–Meyer–Sievers (TMS) model [12,16].

The present work is to investigate a polyamide thin-film composite NF membrane (AFC 30) characterized by modelling of uncharged solutes. The respective experiments were performed to find the rejections of different uncharged solutes and the data obtained interpreted in order to determine the structural characteristics of AFC 30 membrane (effective pore size and thickness-to-porosity ratio) by the Donnan steric partitioning model (DSPM). Also, the charge properties of membrane surface were found from the rejection experiments with solutions of sodium chloride at different concentrations using the Spiegler–Kedem model (SK) in conjunction with TMS model.

Theory

Nanofiltration Transport and Concentration Polarisation

By measuring the solute concentrations in the feed (concentrate solution and also the permeate solution), the separation process by nanofiltration is evaluated *via* calculating the rejection observed as follows

$$R_0 = 1 - \frac{C_{i,\mathrm{p}}}{C_{i,\mathrm{f}}} \tag{1}$$

In nanofiltration processes, the pressure applied on the feed side of the membrane allows solvent to flow through the membrane pores, which is accompanied by a partial permeation of the solutes. Therefore, the solutes retained by the NF membrane are accumulated near the membrane surface, which makes the solutes concentration in the bulk of the feed ($C_{i,\mathrm{f}}$) different from that of the solutes due to the boundary formed in the proximity of the membrane surface ($C_{i,\mathrm{m}}$). This phenomenon is called concentration polarisation, and basically described by the film theory [17-20]. By using the film layer model for concentration polarisation, the solute concentration in the vicinity of the membrane surface can be expressed as follows

$$C_{i,\mathrm{m}} = C_{i,\mathrm{p}} + \left(C_{i,\mathrm{f}} - C_{i,\mathrm{p}}\right)\exp\frac{J}{k} \tag{2}$$

From Eq. (2), the real (intrinsic) rejection can be derived from the following equation

$$R_{\mathrm{r}} = 1 - \frac{C_{i,\mathrm{p}}}{C_{i,\mathrm{m}}} \tag{3}$$

where $C_{i,\mathrm{p}}$ is the solute concentration in permeate, $C_{i,\mathrm{m}}$ the solute concentration in feed solution at the membrane interface (wall), J the permeate volume flux, and k is the mass transfer coefficient in the polarization layer that can be calculated from the well-known Sherwood relationship with Deissler correlation [19]

$$Sh = 0.023\,Re^{0.875}Sc^{0.25} \tag{4}$$

In equations, the Reynold (*Re*), Schmidt (*Sc*) and Sherwood (*Sh*) numbers are given as

$$Re = \frac{u\rho d_{\mathrm{h}}}{\eta} \qquad Sc = \frac{\eta}{\rho D_{i,\infty}} \qquad \text{and} \qquad Sh = \frac{kd_{\mathrm{h}}}{D_{i,\infty}} \tag{5}$$

where u is the fluid velocity in the channel with hydraulic diameter, d_h (the diameter of the tubular membrane in our case), $D_{i,\infty}$the diffusion coefficient of solute i, η and ρ are then the dynamic viscosity and density of the aqueous solution, respectively.

Characterization of Membrane by Using Uncharged Solutes Rejection (DSPM)

The NF membrane can be modelled by considering the membrane as bundles of cylindrical pore radius r_p and length Δx (with $\Delta x \gg r_p$) or as a bundle of slits with length and a half width. The structural parameters, namely the effective pore size (r_p) and the membrane thickness-to-porosity ratio ($\Delta x/A_k$) were estimated through independent experiments of uncharged solutes rejections by considering both slit-like and cylindrical pore geometries. In NF membrane, the rejection of uncharged solutes can only be determined by steric mechanism (size based exclusion). The pore radius (r_p) and the membrane thickness-to- porosity ratio ($\Delta x/A_k$) can be obtained by the Donnan Steric Partitioning Model (DSPM). This model is calculated by fitting the rejection rates using the following equation [20].

$$R_r = 1 - \frac{C_{i,p}}{C_{i,m}} = 1 - \frac{\Phi_i K_{i,c}}{1 - \left[\left(1 - \Phi_i K_{i,c}\right)\exp(-Pe)\right]} \tag{6}$$

where the steric partitioning coefficient of the solute i, λ_i is the pore size ratio. $K_{i,c}$ and $K_{i,d}$ are the hindrance factors for convection and diffusion having different form according to the pore geometry (cylindrical or slit like pores) [20].

The Peclet number (Pe) is defined by the expression

$$Pe = \frac{K_{i,c} J}{K_{i,d} D_{i,\infty}} \frac{\Delta x}{A_k} \tag{7}$$

where A_k is the membrane porosity and Δx the effective membrane thickness.

The hindrance factors for both diffusion ($K_{i,d}$) and convection ($K_{i,c}$) have different definition for both slit like and cylindrical pore geometries in the respective formulas proposed by Deen [21]. Otherwise, there have been new equations derived by Deen and Dechadilok [22], describing the hindrance factors that are valid for the whole range of solutes-to-pore radius ($0 \leq \lambda_i < 1$) of different pore geometries. These equations can be found in Table I.

Table I Hindrance factors for diffusion and convection [22]

Slit-like pores	Cylindrical pores
$\phi_i = 1 - \lambda_i$	$\phi_i = (1 - \lambda_i)^2$
$\lambda_i = \frac{r_{i,s}}{r_p}$	$\lambda_i = \frac{r_{i,s}}{r_p}$
Diffusion	Diffusion
$K_{i,d} = \frac{H(\lambda_i)}{\phi_i}$	$K_{i,d} = \frac{H(\lambda_i)}{\phi_i}$
$H(\lambda_i) = 1 + \frac{9}{8}\lambda_i \ln\lambda_i - 1.19358\lambda_i + 0.4285\lambda_i^3 - 0.3192\lambda_i^4 + 0.08428\lambda_i^5$	$H(\lambda_i) = 1 + \frac{9}{8}\lambda_i \ln\lambda_i - 1.56034\lambda_i + 0.528155\lambda_i^2 + 1.91521\lambda_i^3 - 2.81903\lambda_i^4 + 0.270788\lambda_i^5 + 1.10115\lambda_i^6 - 0.435933\lambda_i^7$
Convection	Convection
$K_{i,c} = \frac{W(\lambda_i)}{\phi_i}$	$K_{i,c} = \frac{1 + 3.867\lambda_i - 1.907\lambda_i^2 - 0.834\lambda_i^3}{1 + 1.867\lambda_i - 0.741\lambda_i^2}$
$W(\lambda_i) = 1 - 3.02\lambda_i^2 + 5.776\lambda_i^3 - 12.3675\lambda_i^4 + 18.9775\lambda_i^5 + 15.21185\lambda_i^6 - 4.8525\lambda_i^7$	

Also, the thickness-to-porosity ratio $\Delta x/A_k$ from the water flux can be found using the Hagen–Poiseuille equation for different pore geometries

$$J_w = L_p \Delta P = \frac{R_p^2}{8\eta(\Delta x/A_k)}\Delta P \quad \text{for cylindrical pores} \tag{8}$$

$$J_w = L_p \Delta P = \frac{R_p^2}{3\eta(\Delta x/A_k)}\Delta P \quad \text{for slit-like pores} \tag{9}$$

where J_w is the pure water flux, L_p the pure water permeability, ΔP the transmembrane pressure and η is the solution viscosity.

By incorporating the expression for the thickness-to-porosity ratio into the Peclet number equation, a new expression is obtained for real rejection, depending only on the pore radius. By fitting the experimental retention value for different pressures with the real rejection equation, the pore radius can then be estimated. This is followed by the corresponding values for the membrane thickness-to-porosity ratio. Since $\Delta x/A_k$ is the parameter of the active layer, the application of these equations means that the pressure drop is negligible through the whole

microporous sublayer, implying that the trans-membrane pressure drop can be attributed to the active layer, which is an assumption made in most literature [15].

Spiegler–Kedem Model (SKM)

The Spiegler–Kedem model is a well-known irreversible thermodynamics (IT) model used to describe the single solutes and solvent in both NF and RO processes [20].This model describes the membrane as a black box, and the solvent and solute transport is defined by a sum of convective (due to the pressure gradient) and diffusive (due to the concentration difference existing at the membrane sides) fluxes. The three transport coefficients which satisfy the Spiegler–Kedem model are: the reflection coefficient (σ), the solute permeability (ω), and the water permeability (L_p). By applying a linear relationship on a local level, the following equations can be written

$$J_v = L_p(\Delta P - \sigma\Delta\pi) \tag{10}$$

$$J_i = \omega\Delta C_{i,m} + (1 - \sigma)J_v C_{i,m} \tag{11}$$

where J_v is the solvent is flux and J_i the solute flux.

Equation (11) is an expression of the well-known Spiegler–Kedem equation (in the integrated form). The salt rejection R at different volumetric flow rates J_v can be calculated as

$$R = \frac{\sigma(1 - F)}{1 - \sigma F} \quad \text{with} \quad F = \exp\left(-\frac{1 - \sigma}{\omega}\right) J_v \tag{12}$$

Teorell–Meyer–Sievers Model (TMS)

The Teorell–Meyer–Sievers model which is also called the fixed charge describes the transport characteristics of solutes through the NF membrane via the electrical properties [7,16]. It explains that the transport of charged solutes through the membranes is accomplished only by the electrostatic effects. The TMS model thus assumes that the fixed charge in the porous NF membrane is distributed uniformly [23]. In addition, these electrical properties served to find the effective fixed charge density of the membrane (ΦX).

Since is a salt solution of a 1-1 type electrolyte and a negative charged NF membrane, the TMS-model equations involving the reflection coefficient (σ) and solute permeability (ω) are given by the following relations [12]

$$\sigma = 1 - \frac{2}{(2\alpha - 1)\xi + (\xi^2 + 4)^{0.5}} \quad (12)$$

$$\omega = D_s(1 - \sigma)\frac{A_k}{\Delta x} \quad (13)$$

where ξ is the parameter which expresses the electrostatic effects being defined as the ratio of the fixed charge density of the membrane (X) to the concentration of the 1-1 electrolyte *(C)*.

The transport number of a cation in the free solution (α) and the diffusivity of the 1-1 electrolyte (D_s) found in Eqs (13) and (14) are then calculated from diffusion coefficients of the individual ions by using these equations

$$\alpha = \frac{D_{+,\infty}}{D_{+,\infty} + D_{-,\infty}} \quad (14)$$

$$D_s = \frac{2D_{+,\infty}D_{-,\infty}}{D_{+,\infty} + D_{-,\infty}} \quad (15)$$

It is quite known that, for most membranes, the fixed charge density varies with the concentration of the electrolyte used. Therefore, in order to interpret the relationship between the fixed charge density and the concentration of the electrolyte *(C)*, the effective fixed charge density is used instead of X [3,23,24].

Experimental

Materials

A tabular thin film composite NF, AFC 30 (PCI membrane system) was used in our study. It consists of an aromatic polyamide skin layer on a polysulfone substrate. The membrane is capable of withstanding the pressure up to 60 bars, temperature below 60 °C and a pH value in the range of 1.5-9.5. All the reagents used were of analytical reagent grade. The aqueous solution was prepared by dissolving the following reagents: sodium chloride, glucose, glycerol, triethylene glycol (TEG), and lactose; the latter being supplied by Penta (the Czech Republic). The individual solutions were prepared by dissolving the respective reagents in highly demineralised water (with conductivity < 1 μS cm^{-1}, pH 6.0 ± 0.2).

Membrane Test Unit

Nanofiltration experiments were performed in a cross-flow separation unit whose scheme is depicted in Fig. 1. A tubular MIC-RO module manufactured from a PCI membrane system was used to carry out the experiment(s). The module was equipped with two tubular AFC 30 NF membranes of 1.25 cm in inner diameter and 30 cm long; the effective filtration area being 240 cm^2.

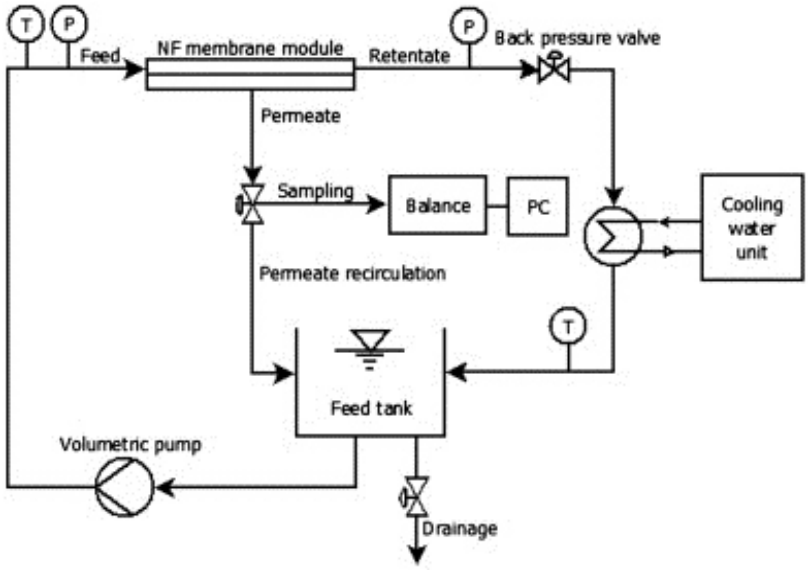

Fig. 1 Setup of nanofiltration experimental system

The experiments were done at a constant temperature of the feed solution of 25 °C and feed volumetric flow of 9 l min^{-1}; transmembrane pressure varying in the range of 5-30 bar. The flux of pure water was measured at various trans-membrane pressures at the same range and the membrane permeability for pure water estimated. The value obtained for permeability of pure water was L_p = 5.84 l m^{-2} h^{-1} bar^{-1} at 25 °C. The NF experiments were performed in the total recycle mode, for both permeate and retentate returning them into the feed tank to maintain a constant concentration in feed. The permeate flux was determined by weighing with electronic balance connected to a personal computer, and samples of permeate and feed collected at each transmembrane pressure. The structural parameters of the membrane, i.e. the effective pore radius (r_p) and the membrane thickness-to-porosity ratio ($\Delta x/A_k$) can be obtained from the uncharged solutes rejection values. The experiment was performed with solutions made 500 mg l^{-1} in concentration and containing glycerol (MW = 92.1 g mol^{-1}), triethylene glycol (MW = 150 g mol^{-1}), glucose (MW = 189 g mol^{-1}), and lactose (MW = 340 g mol^{-1}) at the original pH of demineralized water (6.0 ± 0.2). The concentration of uncharged solutes in feed and permeate was determined by the total organic carbon (TOC) technique.

The membrane surface charge is another parameter which is necessary for characterization of a membrane. It was estimated by carrying out the permeation experiments of NaCl solution at different concentrations from 100-4 500 mg l^{-1} at pH 6.0. Conductivity measurements were done by WTW Cond 340i conductometer (WTW, Germany) equipped with a WTW TetraCon 325 electrode until the permeate conductivity reached the steady state conditions.

In order to assure the reproducibility of the results, the experiments were performed in duplicate. The results obtained represented an average of two identical experiments; the relative standard deviation being up to 5 %. As the membrane characteristics were obtained via the fitting models, the quality of such a fitting was attained by calculating the coefficient of determination (R^2) and the non-linear chi-square test (χ^2), when using the following relationship [25].

$$\chi^2 = \sum \frac{(R_{exp} - R_{cal})^2}{R_{cal}} \tag{16}$$

where R_{exp} and R_{cal} represent the real rejections experimentally determined and calculated in accordance with the models, respectively. Very high values of R^2 indicate a good agreement between the experimental values and theoretical model.

Results and Discussion

Estimation of the Membrane Structure Parameters

The NF experiments for the membrane structural characterization of AFC 30 were performed with uncharged solutes, such as solution of glycerol, triethylene glycol (TEG), glucose and lactose; all having the same concentration of 100 mg l^{-1}. The pure water flux and the fluxes of the solutions used against the pressure difference are shown in Fig. 2.

Data from Fig. 2 indicate that the measured permeate flux as a function of the pressure difference for the uncharged solutes used are similar to the flux of pure water irrespective of the solutes. This shows that the osmotic pressure of the solution is negligible and the variations of typical properties (density, viscosity and diffusion coefficients) can be omitted. As the fluxes of the uncharged solutes are considered to be identical to those for pure water, no fouling was found in our case. Such assumptions are useful for diluted solutions. It has been observed that the flux linearly increases with the increased pressure difference. Such solute rejections increased continuously (below 20 bar) for uncharged solutes, which can be seen in Fig. 3. From our results, the molecular weight cut-off (MWCO) being 90 % of solutes retained by the membrane is between the maximum observed for

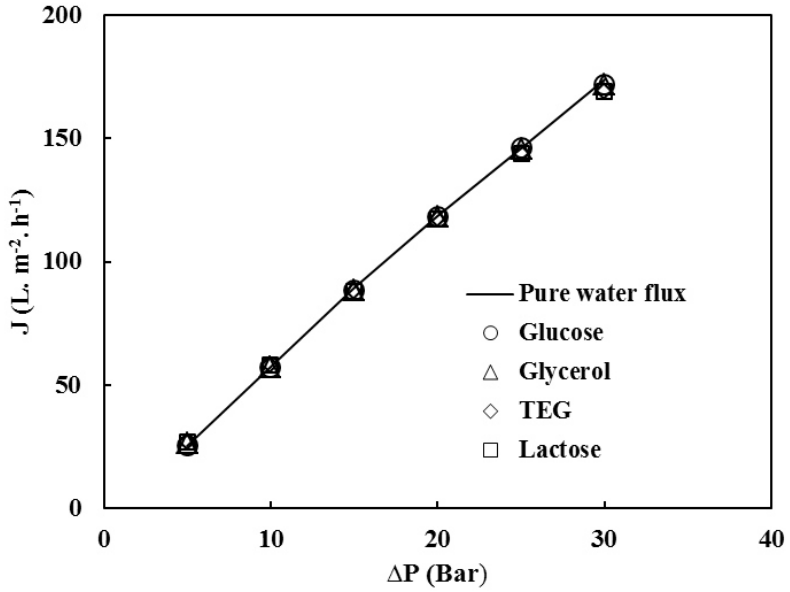

Fig. 2 Comparison of pure water flux and the permeate fluxes of uncharged solutes

rejection of triethylene glycol and glucose as illustrated in Fig. 3. Thus, we can assume that the molecular weight cut-off (MWCO) of AFC 30 is approximately 150 g mol^{-1} (when using interpolation between TEG and glucose resulting in 153 g mol^{-1}).

The real rejections for 500 mg l^{-1} solution of uncharged solutes are plotted against the flux by AFC 30 membrane. It can be observed that, as the molecular weight of the uncharged solutes (as seen in Table II) increases, the real rejection increases, which is seen in Fig. 4.

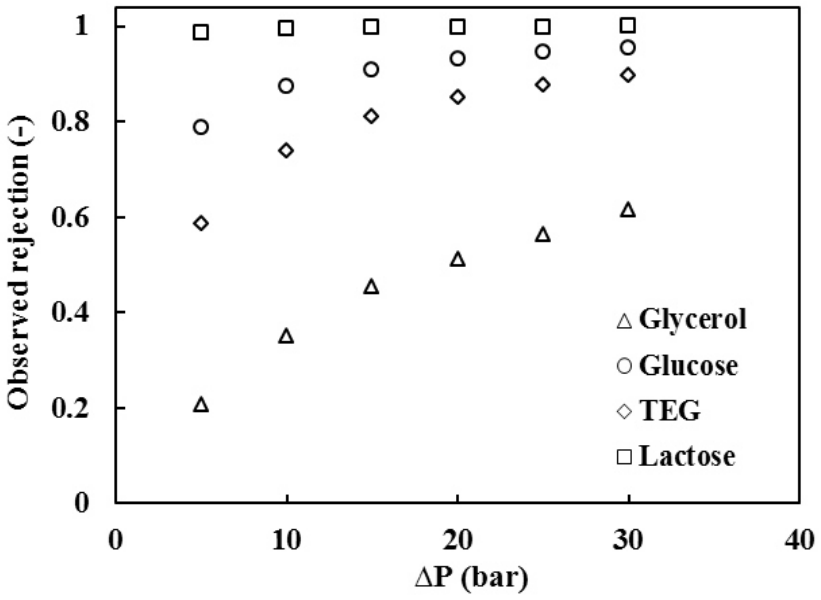

Fig. 3 Influence of operating trans-membrane pressure difference on the rejection observed experimentally

The membrane parameters (the pore radius and thickness to porosity) shown in Table II have been obtained by fitting r_p into Eq. (6) and then by calculating the $\Delta x/A_k$ ratio from Eq. (8). Table III and Fig. 4 then together show that Eq. (6) describes our experimental values very well for all the uncharged solutes used. Very small values obtained for non-linear parameters χ^2 are a confirmation for this. The pore radius and membrane thickness-to-porosity parameter were determined by considering the AFC 30 membrane modelled as a bundle of cylindrical pores. Pore sizes were similar, irrespective of the uncharged solutes; their average values obtained being $r_p = 0.51$ nm and $\Delta x/A_k = 2.23$ μm.

This means that an uncharged solute can be used to determine the pore radius and membrane porosity ratio without experiment, but using different uncharged solutes. In addition, the experimental and rejections calculated from the average value of pore size are in good agreement as shown in Fig. 4. Other study has found a similar pore size of 0.55 nm and the membrane thickness-to-porosity ratio as 2.43 μm [26].

Membrane Charge Density

The membrane charge is an important parameter useful in the NF process. This is due to the fact that the separation mechanism is a combination of size exclusion and electrical interaction (repulsion forces) between the ions in the feed (retentate) and the charged membrane. In addition, the membrane charge allows one to estimate, explain, and model the respective NF processes.

Table II Characteristics of the AFC 30 membrane structural parameters calculated by using DSPM model

Solute	Molar weight g mol^{-1}	Diffusivity $\times 10^{10}$ m^2 s^{-1}	Stokes radius nm	Membrane structural parameters		Quality of fitting r_p χ^2
				r_p, nm	$\Delta x/A_k$, μm	
Glycerol	92.1	9.5	0.26	0.49	2.08	9.14×10^{-3}
TEG	150	7.3	0.34	0.51	2.3	1.64×10^{-2}
Glucose	189	6.7	0.36	0.49	2.05	8.42×10^{-3}
Lactose	340	4.9	0.50	0.53	2.48	1.51×10^{-4}
				0.51	2.23	
				(Average)		

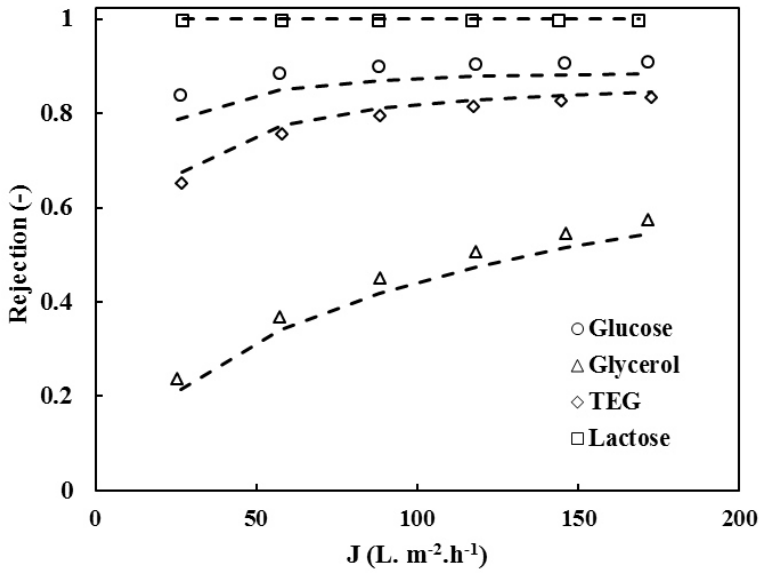

Fig. 4 Comparison between real rejection at the pores with average radius of 0.51 nm (dashed lines) and rejection observed based on experimental data (symbols)

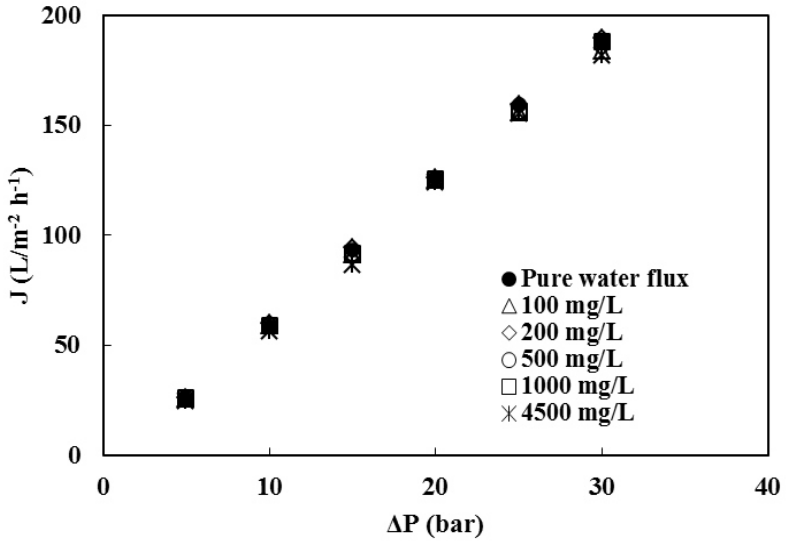

Fig. 5 Pure water flux and fluxes of NaCl solutions with different concentrations (from 100-4 500 mg l^{-1})

The membrane charge is determined by the type or chemical structure of the membrane material, and is due to the dissociation of the functional group(s) present in the membrane material, or an adsorption of different charge or polarizable solutes from the solution [3]. The AFC 30 membrane has a polyamide outer layer, which gives rise the formation of ammonium ($–NH_3^+$) and carboxyl (–COOH) groups. The isoelectric point of the AFC 30 membrane is at pH about 5.3 in KCl solution. This membrane has similar behavior like the AFC 40 and AFC 80 membrane [27]. If the pH < IEP the membrane is positively charged as the carboxyl groups are non-dissociated and the amino groups protonated. Likewise,

the membrane bears negative charge at pH > IEP as the carboxyl groups are dissociated.

To estimate the membrane charge, different experiments were performed for NaCl solutions varying in concentrations in an interval of 100-4 500 mg l^{-1}. Figure 5 depicts the water flux and the permeate fluxes against the pressure applied to the salt solutions. It has been observed that the permeate flux slightly decreases with the increase of NaCl concentration, which can be explained as a result of the increased osmotic pressure.

The reliance of real rejection against the permeate volume flux for NaCl solutions at different concentrations is presented in Fig. 6. The salt diffusivity D_s = 1.61×10^{-9} m^2 s^{-1} was used to analyze the real rejections by means of Eq. (16), accomplished by considering the diffusion coefficients of the individual ions: D_{∞,Na^+} = 1.33×10^{-9} m^2 s^{-1} and D_{∞,Cl^-} = 2.03×10^{-9} m^2 s^{-1} [28].

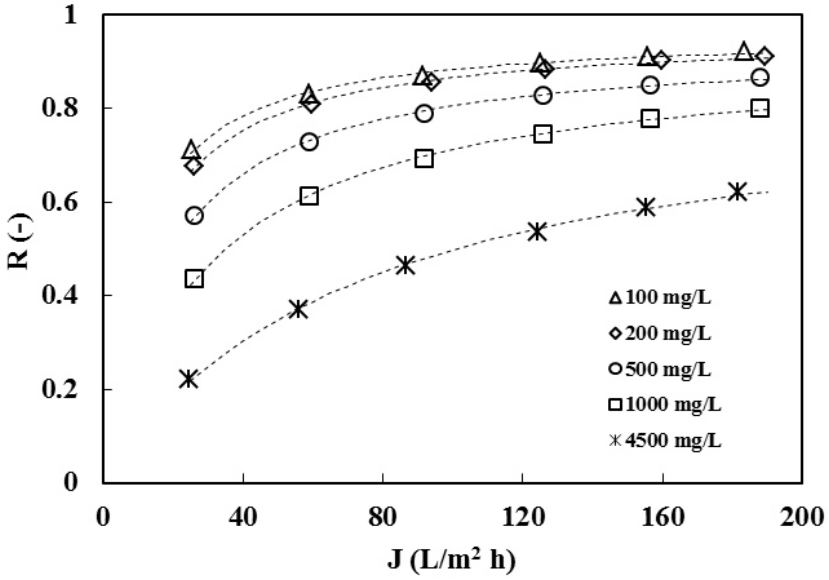

Fig. 6 Rejection of NaCl by the AFC 30 membrane in dependence of the flux. Experimental points were fitted by Spiegler–Kedem model (dashed lines)

As depicted in Fig. 6, the solute rejections gradually decrease with the increasing of NaCl concentration in the feed solution. Meanwhile, trans-membrane pressure extensively increases with the solute rejection for all the concentrations of NaCl during experiments. Salt rejections (denoted by symbols) in the experiments were fitted with the Spiegler–Kedem model (dashed lines). Fig. 6 documents good agreement between the model and experimental data and the values of model parameters (the reflection coefficient and solute permeability) can then be found in Table III.

The TMS model in Eq. (13) can be simplified, when the transport number of cation in the free solution (α) is constant and calculated as 0.3954 (from Eq. (15)). When this value is inserted into the TMS model, one can achieve further

simplification to a quadratic equation that is valid specifically for sodium chloride and can be written as follows

$$0.9562\xi^2 + \frac{0.8371\xi}{\sigma - 1} + 4 - \left(\frac{2}{\sigma - 1}\right)^2 = 0 \qquad (18)$$

The value of the effective fixed charge density have been calculated from Eq. (18) based on the reflection coefficient for each NaCl concentration; the respective reflection coefficient(s) computed via the by Spiegler–Kedem model; see Table III.

Both positive and negative values for the resulting charge could be obtained using Eq. (18); the negative values being used because of a physical meaning that the membrane is charged negatively.

Table III Reflection coefficients (σ) and solute permeabilities (ω) determined by fitting experimental data of NaCl rejection by means of the Spiegler–Kedem model

NaCl concentration mg l^{-1}	Spiegler–Kedem model parameters		Effective fixed charge density $-\Phi X$, mV	Quality of fitting χ^2
	σ	ω, m^{-2} h^{-1}		
100	0.940	9.07	48.8	1.23×10^{-4}
200	0.936	10.97	87.9	9.25×10^{-5}
500	0.903	16.59	144.0	1.08×10^{-4}
1000	0.873	28.37	211.2	1.30×10^{-4}
4500	0.781	67.30	564.0	4.15×10^{-4}

Data seen in Fig. 6 and Fig. 7, as well as the values of the non-linear parameter χ^2 in Table III depict that the Spiegler–Kedem model describes satisfactorily the experimental rejection data for all the concentrations of NaCl considered.

As seen in Fig. 6, the reflection coefficient (σ) decreases and the solute permeability (ω) increases with the increasing concentration of the salt in the feed solution. This is in good agreement with the gradually decreasing rejection with higher concentrations of NaCl in solutions as ascertained experimentally (Fig. 6).The Spiegler–Kedem model then corresponds well to experimental results for the rejection of NaCl.

The dependence of the effective fixed charge density (ΦX) of AFC 30 membrane can be seen in Fig. 7 which is an estimate from Eq. (18) for various concentrations of NaCl in the feed solution. It has been observed that the membrane charge is strongly dependent on the concentration in the feed solution

which had been in contact to the membrane. The membrane charge was increasing with higher concentrations of NaCl in the solution. Other authors have noticed a similar trend that can be attributed to spontaneous adsorption of ions from the solution at the membrane surface [3,5,8,17,23]. Thus, from experimental results, the increase in the negative membrane charge can be explained by adsorption of the chloride ions onto the membrane.

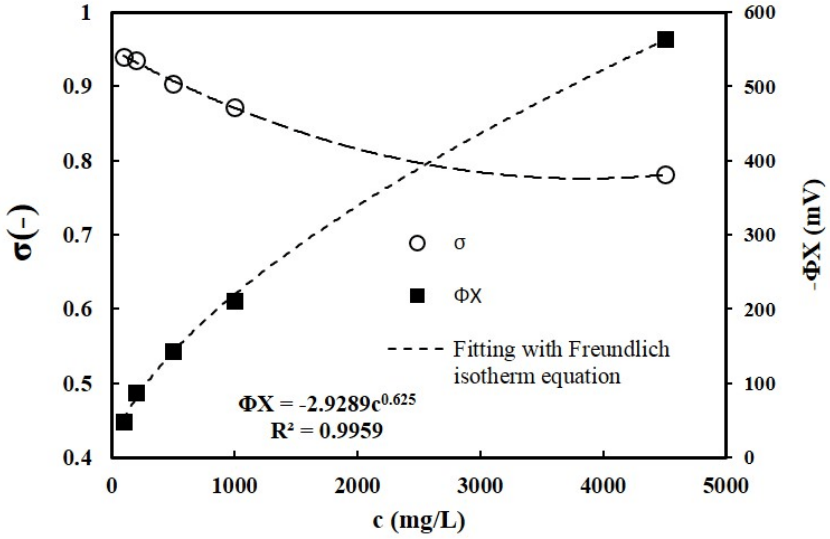

Fig. 7 Reflection coefficient and effective fixed charge density of the AFC 30 membrane as a function of NaCl concentration in the feed solution. Effective charge density was fitted with the Freundlich isotherm (dashed line)

Conclusion

In this study, the complete characterization of the AFC 30 NF membrane was performed by modelling of the respective rejection experiments. The Donnan steric partitioning pore model (DSPM) for uncharged solutes has been confirmed useful for determining typical structural properties — the pore radius (r_p) and the membrane thickness-to-porosity ($\Delta x/A_k$). The structural characterization has revealed that the AFC 30 membrane had effective pore radius of 0.51 nm and the thickness-to-porosity ratio 2.23 μm, respectively. The electrical properties; i.e., the fixed charge density have then been estimated from the rejections experiments with solutions of NaCl at various concentrations by using the Spiegler–Kedem and Teorell–Meyer–Sievers (TMS) models. As found out, the charge density of the membrane was dependent solely on the concentration of the electrolyte solution. This means that the charge density has gradually increased with the increasing concentration of solution(s), which can be described by the Freundlich isotherm. The chloride ions from the solution are absorbed preferably on the membrane surface, thus increasing the membrane negative charge.

Acknowledgement

E. W. would like to thank the Ministry of Education, Youth and Sports of the Czech Republic for financial support under the project SGS_2017_002.

Symbols

A_k membrane porosity
$C_{i,f}$ concentration of solute *i* in feed solution, mol m^{-3}
$C_{i,m}$ concentration of solute *i* in feed solution at membrane surface, mol m^{-3}
$C_{i,p}$ concentration of solute *i* in permeate solution, mol m^{-3}
$c_{i,m}$ concentration of solute *i* in membrane, mol m^{-3}
$D_{i,\infty}$ bulk diffusivity of solute *i*, $m^2 s^{-1}$
d_h hydraulic diameter, m
J permeate volume flux, $m^3 m^{-2} s^{-1}$
J_w pure water flux, $m^3 m^{-2} s^{-1}$
k mass transfer coefficient in polarization layer, m s^{-1}
$K_{i,c}$ hindrance factor for convection
$K_{i,d}$ hindrance factor for diffusion
L_p permeability of pure water, m s^{-1} Pa^{-1}
$r_{i,s}$ Stokes radius of component *i*, m
r_p pore radius, m
Pe Peclet number
R_r real (intrinsic) rejection
R_o observed rejection
Re Reynolds number
Sc Schmidt number
Sh Sherwood number
u fluid velocity in channel, m s^{-1}

Greek Symbols

ΔP trans-membrane pressure difference, bar
η dynamic viscosity, Pa s
ρ density, kg m^{-3}
ϕ_i steric partitioning coefficient of solute *i*
λ_i solute *i* to pore size ratio

References

[1] Mohammad A.W., Teow Y.H., Ang W.L., Chung Y.T., Oatley-Radcliffe D.L., Hilal N.: Desalination **356**, 226 (2015).
[2] Pandya J.A.: Chemical engineering department, GCET. Er. No. 14110730001 (2015).
[3] Gherasim C.V, Mikulášek P., Chýlková J., Krejčová A.: Sci. Pap. Univ. Pardubice, Ser. A **20**, 343 (2014).
[4] Gherasim C.V., Cuhorka J., Mikulášek P.: J. Membr. Sci. **436**, 132 (2013).
[5] Scheap J., Vandecasteele C., Mohammad A.W., Bowen R.: Sep. Sci. Technol. **34**, 3009 (1999).
[6] Mulder M.: *Basic Principles of Membrane Technology,* 2nd ed., Kluwer Academic Publishers (1996).
[7] Wang X.L., Tsuru T., Nakao S., Kimura S.: J. Membr. Sci. **135**, 23 (1997).
[8] Bowen W.R., Mukhtar H.: J. Membr. Sci. **112**, 263 (1996).
[9] Bowen W.R., Welfoot J.S.: Chem. Eng. Sci. **57**, 1121 (2002).
[10] Zhang X., Zhang L., Lu X., Du M.: J. Chem. Eng. **58**, 234 (2007).
[11] Spiegler K.S., Kedem O.: Desalination **1**, 311 (1996).
[12] Wang X.L., Tsuru T., Togoh M., Nakao S., Kimura S.: J. Chem. Eng. Jpn. **28**, 187 (1995).
[13] Szymczyk A., Aoubiza B., Fievet P., Pagetti J.: J. Colloid. Interf. Sci. **216**, 285 (1999).
[14] Szymczyk A., Fievet P.: Desalination **200**, 122 (2006).
[15] Lanteri Y., Szymczyk A., Fievet P.: Langmuir **24**, 7955 (2008).
[16] Hoffer E., Kedem O.: Desalination **2**, 25 (1967).
[17] Zydney A.L.: J. Membr. Sci. **130**, 275 (1997).
[18] Bowen W.R., Mohammad A.W.: AIChE J. **44**, 1799 (1998).
[19] Diessler R.G.: *Analysis of Turbulent Heat Transfer, as Transfer and Friction in Sooth Tubes at High Prandth and Schidt Numbers*, National Advisory Committee for Aeronautic (NACA) Rep. 1210 (1995).
[20] Cavaco Morãoa A.I., Szymczyk A., Fievet P., Alves A.: J. Membr. Sci. **322**, 320 (2008).
[21] Deen W.M.: AIChE J. **33**, 1409 (1987).
[22] Dechadilok P., Deen W.M.: Ind. Eng. Chem. Res. **45**, 6953 (2006).
[23] Wang X. L., Fang Y. Y., Tu C. H., Van der Bruggen B.: Int. Phys. Chem. **31**, 114 (2012).
[24] Kobatake Y., Takeguchi N., Toyoshima Y., Fujita H.: J. Phys. Chem. **69**, 3981 (1965).
[25] Foo K.Y., Hameed B.H.: Chem. Eng. J. **156**, 2 (2010).
[26] Bouranene S., Fivet P., Szymczyk A., Ei-Hadi Samar M., Vidonne A.: J. Membr. Sci. **325**, 150 (2008).

[27] Mikulášek P., Cuhorka J.: Chem. Eng. Transactions **47**, 379 (2016).
[28] Vanysek P. (Ed.): Electrochemical series. CRC Handbook of Chemistry and Physics, **87** (1998).